

MUSE library of stellar spectra

Valentin D. Ivanov¹, Lodovico Coccato¹, Mark J. Neeser¹, Fernando Selman⁴, Alessandro Pizzella^{2,3}, Elena Dalla Bontá^{2,3}, Enrico M. Corsini^{2,3}, and Lorenzo Morelli⁵

¹ European Southern Observatory, Karl-Schwarzschild-Str. 2, 85748 Garching bei München, Germany

² Dipartimento di Fisica e Astronomia “G. Galilei”, Universit di Padova, Vicolo dell’Osservatorio 3, 35122, Padova, Italy

³ INAF-Osservatorio Astronomico di Padova, Vicolo dell’Osservatorio 5, 35122, Padova, Italy

⁴ European Southern Observatory, Ave. Alonso de Córdova 3107, Vitacura, Santiago, Chile

⁵ Instituto de Astronomía y Ciencias Planetarias Universidad de Atacama, Copiapó, Chile

Received 2 November 1002 / Accepted 7 January 3003

ABSTRACT

Context. Empirical stellar spectral libraries have applications in both extragalactic and stellar studies, and they have an advantage over theoretical libraries because they naturally include all relevant chemical species and physical processes. During recent years we see a stream of new high quality sets of spectra, but increasing the spectral resolution and widening the wavelength coverage means resorting to multi-order echelle spectrographs. Assembling the spectra from many pieces results in lower fidelity of their shapes.

Aims. We aim to offer the community a library of high signal-to-noise spectra with reliable continuum shapes. Furthermore, the using an integral field unit (IFU) alleviates the issue of slit losses.

Methods. Our library was build with the MUSE (Multi-Unit Spectroscopic Explorer) IFU instrument. We obtained spectra over nearly the entire visual band ($\lambda \sim 4800$ –9300 Å).

Results. We assembled a library of 35 high-quality MUSE spectra for a subset of the stars from the X-shooter Spectral Library. We verified the continuum shape of these spectra with synthetic broad band colors derived from the spectra. We also report some spectral indices from the Lick system, derived from the new observations.

Conclusions. We offer a high-fidelity set of stellar spectra that covers the Hertzsprung-Russell diagram. It can be useful for both extragalactic and stellar work and demonstrates that the IFUs are excellent tools for building reliable spectral libraries.

Key words. atlases – stars:abundances – stars:fundamental parameters – stars:atmospheres – galaxies:stellar content

1. Introduction

Empirical stellar spectral libraries are one of the most universal tools in modern astronomy. They have applications in both extragalactic and in stellar studies. The former include the modelling of unresolved stellar populations (e.g. Röck et al. 2016), matching and removing continua to reveal weak emission lines (e.g. Engelbracht et al. 1998), usage as templates to measure the stellar line-of-sight velocity dispersions in galaxies (Sargent et al. 1977; Krajnović et al. 2015; Johnston et al. 2018; Martinsson et al. 2018; Nedelchev et al. 2019). The stellar applications include measuring stellar parameters such as effective temperatures (e.g. Beamin et al. 2015) and surface gravities (e.g. Terrien et al. 2015) by template matching or indices, measuring radial velocities (e.g. Swan et al. 2016), and verifying theoretical stellar models which sometime are not as good as one may expect. For example, Sansom et al. (2013) found discrepancies in the Balmer lines, suggesting that the theoretical spectral libraries may not be as reliable source of stellar spectra as the empirical ones. The lists of applications given here are by far incomplete.

We can add a number of open issues related to the libraries: the need to derive homogenous and self-consistent stellar parameters of the library stars – right now the stellar parameters are typically assembled from multiple sources. This requires a two step process: first, derive global solutions of stellar parameters $T_{\text{eff}}/\text{[Fe/H]}/\log g$ versus spectral indices, and then to invert

these relations and to derive new uniform set of stellar parameters for all stars (Sharma et al. 2016; Arentsen et al. 2019, e.g.). Another issue is to define optimal indices, most sensitive to one or another stellar parameter (e.g. Cesetti et al. 2013). A particular problem related to galaxy models is the contribution of the AGB stars (e.g. Maraston 2005).

The most widely used theoretical libraries today are the BaSeL (Kurucz 1992; Lejeune et al. 1997, 1998; Westera et al. 2002) and the PHOENIX (Hauschildt et al. 1999; Allard et al. 2012; Husser et al. 2013), but there have been problems with the treatment of molecules, as shown early on by Castelli et al. (1997), that occasionally lead to poorly predicted broad band colors. Among the empirical libraries the work of Pickles (1998) was the most widely used. It includes 131 flux calibrated stars, but for the vast majority of them the resolving power was below $R=1000$, which is relatively low even for extragalactic applications where the intrinsic velocity dispersion of galaxies require $R \sim 2000$ or higher. Other sets of spectra with better quality have become available: ELODIE (Soubiran et al. 1998; Prugniel & Soubiran 2001; Le Borgne et al. 2004), STELIB (Le Borgne et al. 2003), Indo-US (Valdes et al. 2004), MILES (Sánchez-Blázquez et al. 2006), and CaT (Cenarro et al. 2001, 2007). More recently, single order library with a large number of stars was reported by Yan et al. (2018), but it has been obtained with a 3 arcsec fibers of the SDSS spectrograph (Blanton et al. 2017) and therefore does not avoid completely the slit loss problem. Maraston & Strömbäck (2011) incorporated some of the li-

Send offprint requests to: V. Ivanov, e-mail: vivanov@eso.org

braries listed here in a comprehensive stellar population model at high spectral resolution.

The X-shooter Spectral Library (XSL; Chen et al. 2014) is the latest and most comprehensive effort in this direction. At this time only the optical spectra are available. At this time only the Data Release 1 was available. It contains 237 stars and when completed it will cover $0.3\text{--}2.5\mu\text{m}$ range at a resolving power of $R\sim 7000\text{--}11000$. The XSL is a good example of the problems that increasing resolution and multi-order cross-dispersed spectrographs bring in: the synthetic broad band optical (*UBV*) colors agree poorly with the observed colors from the Bright Star Catalog (on average at $\sim 7\%$ level, see Table 5 and Fig. 26 in Chen et al. 2014). The differences are partially related to pulsating variable stars having been observed in different phases. Slit losses are another issue; for many stars that is caused by the lack or the poor quality wide slit observations. Despite these problems, the narrow features in the XSL spectra are self-consistent, e.g. observations in different orders agree well (see Fig. 8 in Chen et al. 2014), and there is a good agreement between features and theoretical models and other empirical libraries (for a comparison with the UVES-POP see Figs. 31–34 in Chen et al. 2014).

In other words, we are facing again a familiar problem: the old theoretical libraries used to predict colors inconsistent with the observations; nowadays, the newest empirical libraries do the same, despite – or because – of the excellent quality of the new data, that made it more apparent. To address this issue we embarked on a project to build a *slitloss-less* empirical spectral library with the MUSE (Multi-Unit Spectroscopic Explorer; Bacon et al. 2010) integral field unit, spanning all major sequences on the Hertzsprung-Russell diagram, with the specific goal of adjusting and verifying the shapes of the spectra in other libraries, both theoretical and empirical. The final product are spectra, suitable for galactic modeling, stellar classification, and other applications. Here we report the first subset of 35 MUSE stellar spectra.

The next two sections describe the sample and the data, respectively. Section 4 presents the analysis of our spectra and Sec. 5 summarizes this work.

2. Sample

Our initial sample numbered 33 targets selected among the XSL stars¹. We aimed to populate the Hertzsprung-Russell diagram as homogeneously as possible with $\sim 3\text{--}6$ bright stars per spectral type, ensuring a high signal-to-noise $S/N>70\text{--}200$ per spectral type, except for the O-type where only a single star was available.

Spectra of two additional stars were obtained: HD 193256 and HD 193281B. They serendipitously fell inside the field of view during the observations of the project target HD 193281A. An IFU campaign covering the entire XSL is planned, but we made sure to select stars over various spectral types, making this trimmed-down library adequate for some applications, such as stellar classification and templates fitting of galaxy spectra.

The SIMBAD spectral types as listed in Chen et al. (2014), and complemented for the two extra targets, together with effective temperatures T_{eff} , surface gravities $\log g$ and metallicities $[\text{Fe}/\text{H}]$ collected from the literature, if available, are listed in Table 1 and shown in Fig. 1². The covered range of T_{eff} is 2600–

33000 K, of $\log g$: 0.6–4.5 and of $[\text{Fe}/\text{H}]$: from -1.22 to 0.55 , as far as the stellar parameters as known. In case multiple literature sources with equal quality were available for a certain parameter, we adopted the average value and if a given source had significantly smaller errors than the others, we adopted the value from that source.

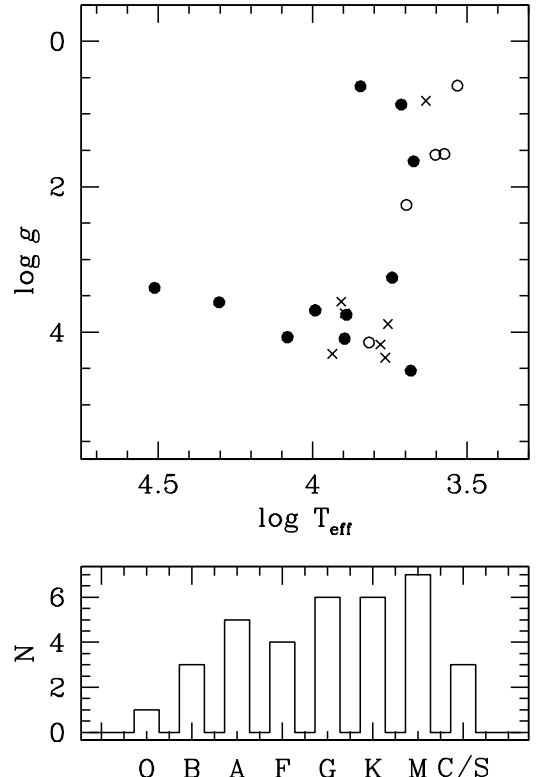


Fig. 1: Properties of the stars in our sample. *Top*: Surface gravity $\log g$ versus effective temperature T_{eff} for stars with $[\text{Fe}/\text{H}]<-0.5\text{ dex}$ (crosses), $-0.5<[\text{Fe}/\text{H}]<0.0\text{ dex}$ (open circles) and $[\text{Fe}/\text{H}]\geq 0.0\text{ dex}$ (solid dots). *Bottom*: Distributions of the stars by spectral type.

3. Observations and Data Reduction

The spectra were obtained with MUSE at the European Southern Observatory (ESO) Very Large Telescope, Unit Telescope 4, on Cerro Paranal, Chile. Table A.1 gives the observing log. We obtained six exposures for each target, except for HD 204155 which was observed 12 times. To maximize the data yield most of the data were obtained under non-photometric conditions, so the absolute flux calibration is uncertain, but the “true” intrinsic shape is preserved, because there is no “stitching” of multiple orders and no variable slit losses due to atmospheric refraction. We placed the science targets at the same spaxels as the spectrophotometric standards, to minimize the instrument systematics that might arise from residual spaxel-to-spaxel variations.

The data reduction was performed with the ESO MUSE pipeline (ver. 2.6) within the ESO Reflex³ environment (Freudling et al. 2013). The 1-dimensional spectra were extracted within a circular aperture with a radius of 6 arcsec. This number was selected after some experiments with apertures of

¹ <http://xsl.u-strasbg.fr/>

² Stellar parameters from XSL also became available after the submission of this paper: Arentsen et al. (2019)

³ <https://www.eso.org/sci/software/esoreflex/>

Table 1: Physical parameters of the program stars. The columns contain: (1) object ID (asterisks mark non-XSL objects); (2) SIMBAD spectral type; (3-4) radial velocity and reference; (4-8) effective temperature, surface gravity, iron abundance and reference. Our estimated spectral type and effective temperature for HD 193281B are also listed.

IDs (1)	Sp. Type (2)	V_{rad} , km s $^{-1}$ (3)	Reference (4)	T_{eff} , K (5)	$\log g$ (6)	[Fe/H] (7)	Reference (8)
HD 057060	O7e...	20.0 \pm 1.7	Pourbaix et al. (2004)	32508 \pm 1928 33215 \pm 2674	3.39 \pm 0.26 3.28 \pm 0.16	0.24 \pm 0.14 −0.03 \pm 0.20	Koleva & Vazdekis (2012) Prugniel et al. (2011)
HD 064332	S	−1.3 \pm 0.5	Gontcharov (2006)	3399 \pm 44	0.61 \pm 0.40	−0.04 \pm 0.18	Prugniel et al. (2011)
HD 067507	CNv...	23 \pm 10	Wilson (1953)	2680	Bergeat et al. (2002)
HD 085405	C	3.50 \pm 1.6	Gontcharov (2006)	2769 2645	...	−0.10 ...	Soubiran et al. (2016) Bergeat et al. (2002)
HD 096446	B2IIIp	6.1 \pm 0.8	Gontcharov (2006)	20086 \pm 530	3.59 \pm 0.08	0.06 \pm 0.04	Koleva & Vazdekis (2012)
HD 099648	G8Iab	−8.82 \pm 0.19	Gaia Collaboration (2018)	4970 \pm 75 4977 \pm 49	2.25 \pm 0.43 2.24 \pm 0.12	−0.01 \pm 0.15 −0.03 \pm 0.06	Koleva & Vazdekis (2012) Prugniel et al. (2011)
HD 099998	K3.5III	18.43 \pm 0.37	Gaia Collaboration (2018)	4001 \pm 32	1.56 \pm 0.20	−0.24 \pm 0.07	Prugniel et al. (2011)
HD 100733	M3III	21.07 \pm 0.29	Gaia Collaboration (2018)	3530	Wright et al. (2003)
HD 306799	M0Iab	−16.38 \pm 0.19	Mermilliod et al. (2008)	3650	Wright et al. (2003)
HD 101712	M3lab	−0.70 \pm 1.23	Mermilliod et al. (2008)	3200	Wright et al. (2003)
HD 102212	M1III	50.28 \pm 0.09	Famaey et al. (2009)	3738 \pm 6	1.55 \pm 0.10	−0.41 \pm 0.05	Koleva & Vazdekis (2012)
HD 114960	K5III	7.35 \pm 0.16	Gaia Collaboration (2018)	4000	Wright et al. (2003)
IRAS 15060+0947	M9III	−8.2 \pm 2.6	Engels & Bunzel (2015)	3281	Gaia Collaboration et al. (2018)
HD 147550	B9V	−24.1 \pm 0.9	Gontcharov (2006)	9830 \pm 279	3.70 \pm 0.66	−0.38 \pm 0.11	Koleva & Vazdekis (2012)
HD 160365	F6III	8.14 \pm 2.31	Massarotti et al. (2008)	6009	Soubiran et al. (2016)
HD 160346	K3V	17.856 \pm 0.784	Kunder et al. (2017)	4808 \pm 65	4.53 \pm 0.22	0.03 \pm 0.10	Koleva & Vazdekis (2012)
HD 163810	G3V	185.99 \pm 0.22	Latham et al. (2002)	5818 \pm 15	4.35 \pm 0.06	−1.20 \pm 0.04	Koleva & Vazdekis (2012)
HD 164257	A0	5.5 \pm 0.9	Gontcharov (2006)	9792 \pm 691	3.70 \pm 2.11	0.41 \pm 0.30	Koleva & Vazdekis (2012)
[B86] 133	M4	44 \pm 5	this work	4637 2645	...	−0.21 ...	Gaia Collaboration et al. (2018), Ivanov et al. (2004)
HD 167278	F2	−14.7 \pm 0.9	Gontcharov (2006)	6563 \pm 18	4.14 \pm 0.08	−0.21 \pm 0.04	Koleva & Vazdekis (2012)
HD 170820	K0III	2.84 \pm 0.06	Mermilliod et al. (2008)	4707 \pm 57	1.65 \pm 0.13	0.17	Prugniel et al. (2011)
HD 172230	A5	−36.8 \pm 0.8	Gontcharov (2006)	7772 \pm 102	3.76 \pm 0.44	0.55 \pm 0.14	Koleva & Vazdekis (2012)
HD 173158	K0	14.06 \pm 0.32	Gaia Collaboration (2018)	5164 \pm 121	0.87 \pm 0.43	0.04 \pm 0.20	Koleva & Vazdekis (2012)
HD 174966	A3	5.6 \pm 0.9	Gaia Collaboration (2018)	7874 \pm 57	4.09 \pm 0.16	0.03 \pm 0.10	Koleva & Vazdekis (2012)
HD 175640	B9III	−26.0 \pm 4.3	Gontcharov (2006)	12067 \pm 326 12077 \pm 453	4.07 \pm 0.55 3.94 \pm 0.21	0.22 \pm 0.18 0.17 \pm 0.15	Koleva & Vazdekis (2012) Prugniel et al. (2011)
HD 179821	G5Ia	81.78 \pm 3.71	Gaia Collaboration (2018)	6997 7107	0.62 1.00	0.44 0.45	Soubiran et al. (2016)
HD 232078	K3IIp	−388.34 \pm 0.27	Soubiran et al. (2008)	4295 \pm 48 4014 \pm 48	0.82 \pm 0.27 0.81 \pm 0.20	−1.08 \pm 0.11 −1.22 \pm 0.11	Koleva & Vazdekis (2012) Prugniel et al. (2011)
HD 193256*	A8Vn...	6 \pm 2	this work	7860	3.74	−0.95	Soubiran et al. (2016)
HD 193281A	A2III	0.3 \pm 0.5	Gontcharov (2006)	8623 \pm 345 8597 \pm 218	4.30 \pm 0.33 4.11 \pm 0.14	−0.68 \pm 0.28 −0.37 \pm 0.13	Koleva & Vazdekis (2012) Prugniel et al. (2011)
HD 193281B*	F5:V:	−43.13 \pm 0.97	Gaia Collaboration (2018)	8080 8080 8414	3.58 3.58 ...	−1.00 −1.00 ...	Soubiran et al. (2016)
HD 193896	K2III			4354 \pm 57	this work
HD 196892	G5IIIa	−15.23 \pm 0.18	Gaia Collaboration (2018)	4900	Wright et al. (2003)
HD 200081	F6V	−34.498 \pm 0.004	Santos et al. (2011)	6028 \pm 22	4.17 \pm 0.10	−0.99 \pm 0.07	Koleva & Vazdekis (2012)
HD 204155	G0	7.67 \pm 0.27	Soubiran et al. (2008)	5526 \pm 71	3.25 \pm 0.43	0.02 \pm 0.12	Koleva & Vazdekis (2012)
	G5	−84.60 \pm 0.16	Latham et al. (2002)	5704 \pm 28 5718 \pm 56	3.89 \pm 0.16 3.93 \pm 0.11	−0.70 \pm 0.07 −0.69 \pm 0.06	Koleva & Vazdekis (2012) Prugniel et al. (2011)
HD 209290	M0.5V	18.144 \pm 0.069	Soubiran et al. (2013)	4031	...	−0.06	Ammons et al. (2006)

difference sizes, to guarantee that “aperture” losses will lead to a change in the overall slope of the spectra $<1\%$ from the blue to the red end. The sky emission was estimated within an annulus of an inner radius 7 arcsec and a width of 4 arcsec. This step of the analysis was performed with an IRAF⁴/PyRAF tool (Tody 1986, 1993; Science Software Branch at STScI 2012).

Three stars were treated differently. For [B86] 133 we reduced the extraction aperture radius to 4 arcsec (keeping the sky annulus the same as for the majority of the targets) to avoid con-

tamination from nearby sources – because the object is located in a crowded Milky Way bulge field. HD 193256 is close to the edge of the MUSE field of view, and the extraction apertures had to be smaller, with a radius 4.6 arcsec, the sky annulus had an inner radius of 4.6 arcsec and a width of 2 arcsec. HD 193281 is a binary with \sim 3.8 arcsec separation and the components cross-contaminate each other. To separate the two spectra we first extracted a combined spectrum of the two stars together with the same aperture and annulus as for the bulk of the stars. Next, we rotated each plane of the data cube by 180° around the centre of the primary and subtracted the rotated plane from the original

⁴ IRAF is distributed by the NOAO, which is operated by the AURA Inc., under contract to the NSF.

non-rotated plane, to remove the contribution of the primary at the location of the secondary. Then, we extracted the spectrum of the secondary with an aperture with a radius of 1.2 arcsec and a sky annulus with an inner radius of 1.8 arcsec and a width of 4 arcsec. Finally, we decontaminated the spectrum of the primary by subtracting the spectrum of the secondary from the combined spectrum of the binary.

Experiments with apertures of different sizes indicated that the continuum shape of [B86] 133 still changed at <1% level across the entire wavelength range, despite the narrower extraction aperture. The spectra of the two other objects are less reliable and in the case of HD 193281B a change in the radius of a few spaxels (0.2 arcsec) leads to a flux change of ~3 % over the entire wavelength range. However, the spectrum of HD 193281A is still stable at <1 % because the secondary contributes ~1 and ~11 % to the total flux at the blue and at the red ends of the spectrum, respectively, so this ~3 % uncertainty is reduced by a factors of ~100 and ~9, respectively, and the spectrum of HD 193281A can be considered reliable by to our criterion for <1% stability across the entire spectral range.

The telluric features were removed by running *molecfit* ver. 1.5.7 (Smette et al. 2015; Kausch et al. 2015) separately on each of the six (12 for HD 204155) target spectra themselves. The agreement of individual solutions is excellent: typically the fits yield a precipitable water estimate identical to within <0.1 mm.

The final spectrum for each target is the average of the 1-D spectra derived from the six individual observations, and the error is the r.m.s. of that averaging. A example of the data products is plotted in Fig. 2. The complete sample is shown in Fig. A.1. All final spectra are given in Table A.2 and are available in machine readable form at the journal's website.

4. Analysis

A direct comparison of the MUSE and XSL spectra for eight randomly selected stars across the spectral type sequence is shown with some zoomed-in spectral regions in Fig. 3 (for the rest of out spectra see Figs. 2 and A.1). Notably, the XSL spectra used the continuum shape from a 5 arcsec wide-slit observaitons. In most cases the agreement on a scale of a few hundred pixels—in other words, within the same X-shooter order—is excellent. However, on wider scale we find deviations between the XSL and MUSE spectra, as can be seen in Fig. 4. The exceptions are usually late type stars – [B86] 133 and IRAS 15060+0947 are examples – where the low signal-to-noise in the blue (~10 or bellow) and the variability that only occurs with extremely red stars may account for the problem. Furthermore, the ratios of many spectra show gradual change, despite of their apparently high signal-to-noise: HD 147550 and HD 167278 are examples where the amplitude of the ratio within the MUSE wavelength range reaches 10–15 %. We fitted to the ratios second order polynomials and extrapolated them over the full wavelength range covered by the XSL library to demonstrate that if these trends hold, the overall peak-to-peak flux differences can easily rich ~20 %, so the overall continuum of the cross-dispersed spectra is somewhat ill-defined. The coefficients of the polynomial fits are listed in Table B.1. and can be used to correct the shape of the XSL spectra. We are far from critisizing Chen et al. (2014) for the quality of their data reduction, rather we point here that the high signal-to-noise observations show how difficult it is to process cross-dispersed spectra. Indeed, problems that may not be obvious with poor quality data become apparent for signal-to-noise if 100–200.

The question remains, however, if the MUSE spectra have a more reliable shape than the XSL spectra, because strictly speaking so far we have only demonstrated the good internal agreement between the six (or 12) individual MUSE observations. To provide and external check we followed Chen et al. (2014), and calculated synthetic SDSS colors from both ours and the XSL spectra (Fig. 5) using the *pyphot* tool⁵. The XSL spectra were median smoothed to remove outliers, e.g. due to poorly removed cosmic ray hits. The MUSE sequences are slightly tighter than the XSL ones, confirming that the MUSE spectra have more reliable shapes. This is expected, because of the slit losses and the imperfect order stitching of the XSL spectra. Furthermore, X-shooter has three arms – in effect, three different instruments, and some of the of the colors mix fluxes from different arms, which may contribute to the larger scatter. A better spectral shape verification will be possible in the future with the *Gaia* low-resolution spectra.

The Lick indices (Worthey et al. 1994) that fall within the wavelength range covered by MUSE were measured in the new spectra (Table C.1). This included: Fe5015, Fe5270, Fe5335, Fe5406, Fe5709, Fe5782, H β , Mg₁, Mg₂, Mg b, NaD, TiO₁ and TiO₂. As designed by our target selection, the measured values occupy the same locus as the Lick library (Fig. 6).

In the course of the analysis we noticed that the Lick indices of HD 193281B correspond to a latter type than the F5:V: reported in Simbad. We derived a new spectral type of K2III using as templates our spectra of HD 170820 and HD 099998 and we adopted for this star the average of their effective temperatures, $T_{\text{eff}}=4354$ K with a tentative uncertainty of 57 K – the larger of the uncertainties of the T_{eff} for these two stars.

The metal features of HD 179821 are stronger than for other stars with similar temperature, but this is probably due to the supersolar abundance of this star (Soubiran et al. 2016). Some Lick indices of late-M and C/S stars also deviate from the locus, but the spectra of these stars are dominated by broad molecular features, making the atomic indices such as Fe, Mg and H, meaningless.

5. Summary and Conclusions

We present high signal-to-noise ($S/N>70$ –200) MUSE spectra of 35 stars across the spectral type sequence. The comparison with higher resolution existing data and spectral index measurements show reasonably good agreement, except for differences in the continuum shape that point at the real difficulties obtaining high-resolution spectra with wide spectral coverage: the instruments that deliver such kind of data spread the light over many orders and their combination is not trivial. Importantly, the integral field unit that we use does not suffer from slit losses.

The sample of spectra presented here is relatively limited in terms of number of stars, and to make this library more useful we need to populate more densely the parametric space. In particular, the metallicity range needs to be expanded. Our data suffer from the high blue wavelength limit of MUSE, missing some important CN, Ca and Fe spectral features in the 4100–4800 Å range. This is a hardware limitation that can only be addressed with other/future instruments. Further accurate broad band photometry is needed to extent the external verification of the continuum shape – so far *Gaia*, SDSS and other photometric surveys provide measurements only for about a quarter of our sample stars – mostly because our program stars are too bright.

⁵ <http://mfouesneau.github.io/docs/pyphot/>

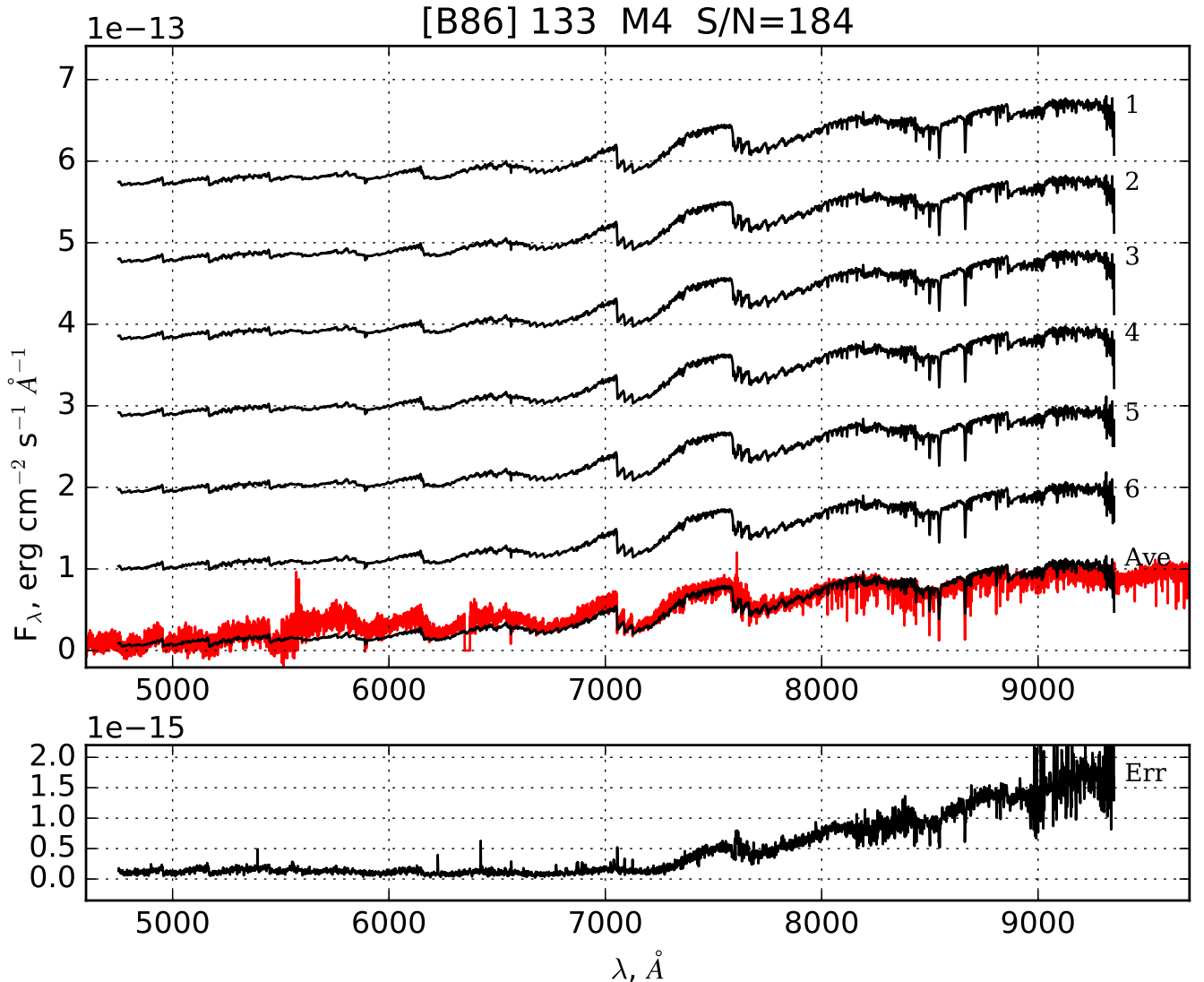


Fig. 2: An example of the MUSE spectra (black line) of [B86] 133 and of the corresponding XSL DR1 spectrum (red line; normalized to match the MUSE spectrum flux). The plot title lists the spectral type and the measured median S/N per resolution element over the entire spectrum. The upper sub-panels show the spectra extracted from each individual exposure (shifted up for clarity) and the average spectra of the object at its true flux level. The bottom sub-panels show the standard deviation of the average spectrum. The spectra of the other sample stars are presented in the electronic edition only (Fig. A.1).

Expanding the MUSE library towards fainter stars will increase this fraction and make such a test statistically significant.

Despite these issues, our MUSE spectral library can be a useful tool for both stellar and galaxy research. This project started as a simple effort to complement the XSL DR1 library, but our spectra can be applied for various MUSE-based research – they have an extra advantage of being obtained with the same instrument so the data format is the same, and any low-level instrumental signatures that might have remained in the data could cancel out. We plan to expand the number of library stars in the future.

Acknowledgements. This paper is based on observations made with the ESO Very Large Telescope at the La Silla Paranal Observatory under program 099.D-0623. We have made extensive use of the SIMBAD Database at CDS (Centre de Données astronomiques) Strasbourg and of the VizieR catalog access tool, CDS, Strasbourg, France. E.M.C., E.D.B., L.M., and A.P. acknowledge financial support from Padua University through grants DOR1715817/17, DOR1885254/18,

DOR1935272/19, and BIRD164402/16. We thank the referee for the comments that helped to improve the paper.

References

- Allard, F., Homeier, D., & Freytag, B. 2012, Philosophical Transactions of the Royal Society of London Series A, 370, 2765
- Ammons, S. M., Robinson, S. E., Strader, J., et al. 2006, ApJ, 638, 1004
- Arentsen, A., Prugniel, P., Gonneau, A., et al. 2019, A&A, 627, A138
- Bacon, R., Accardo, M., Adjali, L., et al. 2010, in Proc. SPIE, Vol. 7735, Ground-based and Airborne Instrumentation for Astronomy III, 773508
- Beamín, J. C., Ivanov, V. D., Minniti, D., et al. 2015, MNRAS, 454, 4054
- Bergeat, J., Knapik, A., & Rutile, B. 2002, A&A, 390, 967
- Blanton, M. R., Bershady, M. A., Abolfathi, B., et al. 2017, AJ, 154, 28
- Castelli, F., Gratton, R. G., & Kurucz, R. L. 1997, A&A, 318, 841
- Cenarro, A. J., Cardiel, N., Gorgas, J., et al. 2001, MNRAS, 326, 959
- Cenarro, A. J., Peletier, R. F., Sánchez-Blázquez, P., et al. 2007, MNRAS, 374, 664
- Cesetti, M., Pizzella, A., Ivanov, V. D., et al. 2013, A&A, 549, A129
- Chen, Y.-P., Trager, S. C., Peletier, R. F., et al. 2014, A&A, 565, A117

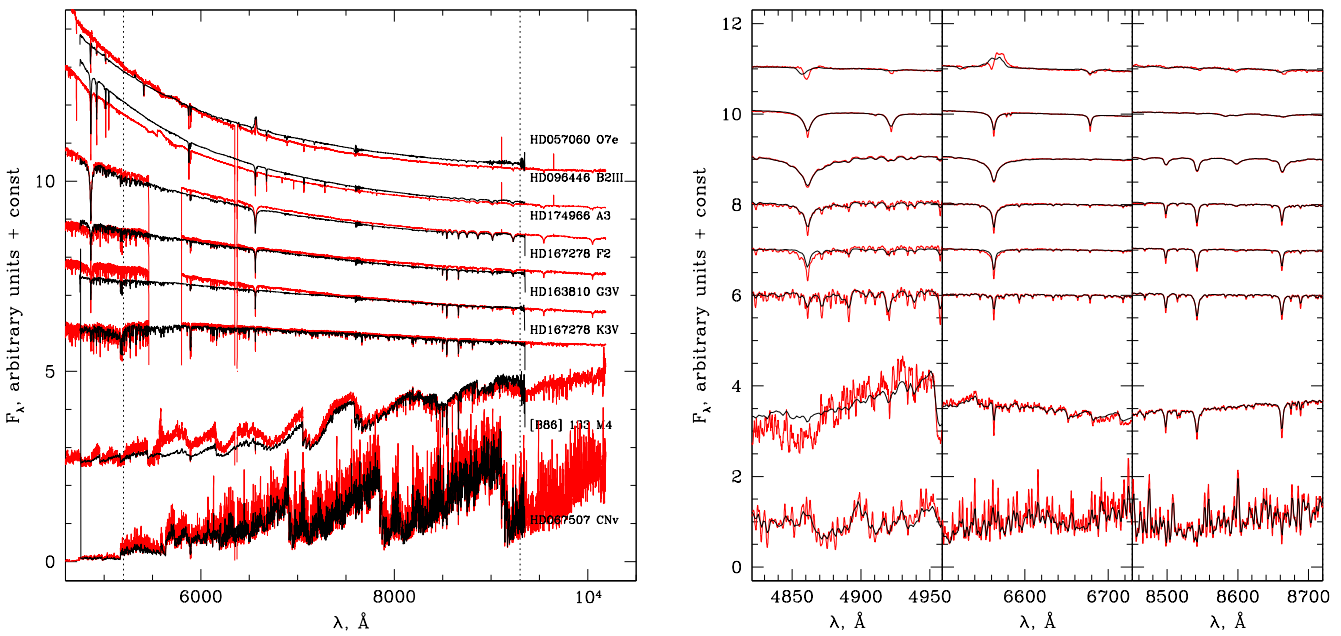


Fig. 3: Comparison of a subset of our MUSE spectra (black lines) with the XSL spectra (red lines; boxcar smoothed over 8 pixels). The spectra are normalized to unity between the two vertical dotted lines shown on the left panel, and shifted vertically for display purposes. The left panel shows the entire MUSE spectral range, the right panel zooms onto the H β , H α , and Ca triplet wavelength ranges (left to right). No radial velocity corrections are applied.

- Engelbracht, C. W., Rieke, M. J., Rieke, G. H., Kelly, D. M., & Achtermann, J. M. 1998, ApJ, 505, 639
 Engels, D. & Bunzel, F. 2015, A&A, 582, A68
 Famaey, B., Pourbaix, D., Frankowski, A., et al. 2009, A&A, 498, 627
 Freudling, W., Romaniello, M., Bramich, D. M., et al. 2013, A&A, 559, A96
 Gaia Collaboration. 2018, VizieR Online Data Catalog, 1345
 Gaia Collaboration, Brown, A. G. A., Vallenari, A., et al. 2018, A&A, 616, A1
 Gontcharov, G. A. 2006, Astronomy Letters, 32, 759
 Hauschildt, P. H., Allard, F., Ferguson, J., Baron, E., & Alexander, D. R. 1999, ApJ, 525, 871
 Husser, T. O., Wende-von Berg, S., Dreizler, S., et al. 2013, A&A, 553, A6
 Ivanov, V. D., Rieke, M. J., Engelbracht, C. W., et al. 2004, ApJS, 151, 387
 Johnston, E. J., Hau, G. K. T., Coccato, L., & Herrera, C. 2018, MNRAS, 480, 3215
 Kausch, W., Noll, S., Smette, A., et al. 2015, A&A, 576, A78
 Koleva, M. & Vazdekis, A. 2012, A&A, 538, A143
 Krajnović, D., Weilbacher, P. M., Urrutia, T., et al. 2015, MNRAS, 452, 2
 Kunder, A., Kordopatis, G., Steinmetz, M., et al. 2017, AJ, 153, 75
 Kurucz, R. L. 1992, in IAU Symposium, Vol. 149, The Stellar Populations of Galaxies, ed. B. Barbuy & A. Renzini, 225
 Latham, D. W., Stefanik, R. P., Torres, G., et al. 2002, AJ, 124, 1144
 Le Borgne, D., Rocca-Volmerange, B., Prugniel, P., et al. 2004, A&A, 425, 881
 Le Borgne, J.-F., Bruzual, G., Pelló, R., et al. 2003, A&A, 402, 433
 Lejeune, T., Cuisinier, F., & Buser, R. 1997, A&AS, 125, 229
 Lejeune, T., Cuisinier, F., & Buser, R. 1998, A&AS, 130, 65
 Lenz, D. D., Newberg, J., Rosner, R., Richards, G. T., & Stoughton, C. 1998, ApJS, 119, 121
 Maraston, C. 2005, MNRAS, 362, 799
 Maraston, C. & Strömbäck, G. 2011, MNRAS, 418, 2785
 Martinsson, T. P. K., Sarzi, M., Knapen, J. H., et al. 2018, A&A, 612, A66
 Massarotti, A., Latham, D. W., Stefanik, R. P., & Fogel, J. 2008, AJ, 135, 209
 Mermilliod, J. C., Mayor, M., & Udry, S. 2008, A&A, 485, 303
 Nedelchev, B., Coccato, L., Corsini, E. M., et al. 2019, A&A, 623, A87
 Pickles, A. J. 1998, PASP, 110, 863
 Pourbaix, D., Tokovinin, A. A., Batten, A. H., et al. 2004, A&A, 424, 727
 Prugniel, P. & Soubiran, C. 2001, A&A, 369, 1048
 Prugniel, P., Vauglin, I., & Koleva, M. 2011, A&A, 531, A165
 Röck, B., Vazdekis, A., Ricciardelli, E., et al. 2016, A&A, 589, A73
 Sánchez-Blázquez, P., Peletier, R. F., Jiménez-Vicente, J., et al. 2006, MNRAS, 371, 703
 Sansom, A. E., Milone, A. d. C., Vazdekis, A., & Sánchez-Blázquez, P. 2013, MNRAS, 435, 952
 Santos, N. C., Mayor, M., Bonfils, X., et al. 2011, A&A, 526, A112
 Sargent, W. L. W., Schechter, P. L., Bokkenberg, A., & Shortridge, K. 1977, ApJ, 212, 326
 Science Software Branch at STScI. 2012, PyRAF: Python alternative for IRAF, Astrophysics Source Code Library
 Sharma, K., Prugniel, P., & Singh, H. P. 2016, A&A, 585, A64
 Smette, A., Sana, H., Noll, S., et al. 2015, A&A, 576, A77
 Soubiran, C., Bienaymé, O., Mishenina, T. V., & Kovtyukh, V. V. 2008, A&A, 480, 91
 Soubiran, C., Jasniewicz, G., Chemin, L., et al. 2013, A&A, 552, A64
 Soubiran, C., Katz, D., & Cayrel, R. 1998, A&AS, 133, 221
 Soubiran, C., Le Campion, J.-F., Brouillet, N., & Chemin, L. 2016, A&A, 591, A118
 Swan, J., Cole, A. A., Tolstoy, E., & Irwin, M. J. 2016, MNRAS, 456, 4315
 Terrien, R. C., Mahadevan, S., Bender, C. F., Deshpande, R., & Robertson, P. 2015, ApJ, 802, L10
 Tody, D. 1986, in Proc. SPIE, Vol. 627, Instrumentation in astronomy VI, ed. D. L. Crawford, 733
 Tody, D. 1993, in Astronomical Society of the Pacific Conference Series, Vol. 52, Astronomical Data Analysis Software and Systems II, ed. R. J. Hanisch, R. J. V. Brissenden, & J. Barnes, 173
 Valdes, F., Gupta, R., Rose, J. A., Singh, H. P., & Bell, D. J. 2004, ApJS, 152, 251
 Westera, P., Lejeune, T., Buser, R., Cuisinier, F., & Bruzual, G. 2002, A&A, 381, 524
 Wilson, R. E. 1953, Carnegie Institute Washington D.C. Publication
 Worthey, G., Faber, S. M., Gonzalez, J. J., & Burstein, D. 1994, ApJS, 94, 687
 Wright, C. O., Egan, M. P., Kraemer, K. E., & Price, S. D. 2003, AJ, 125, 359
 Yan, R., Chen, Y., Lazarz, D., et al. 2018, arXiv e-prints

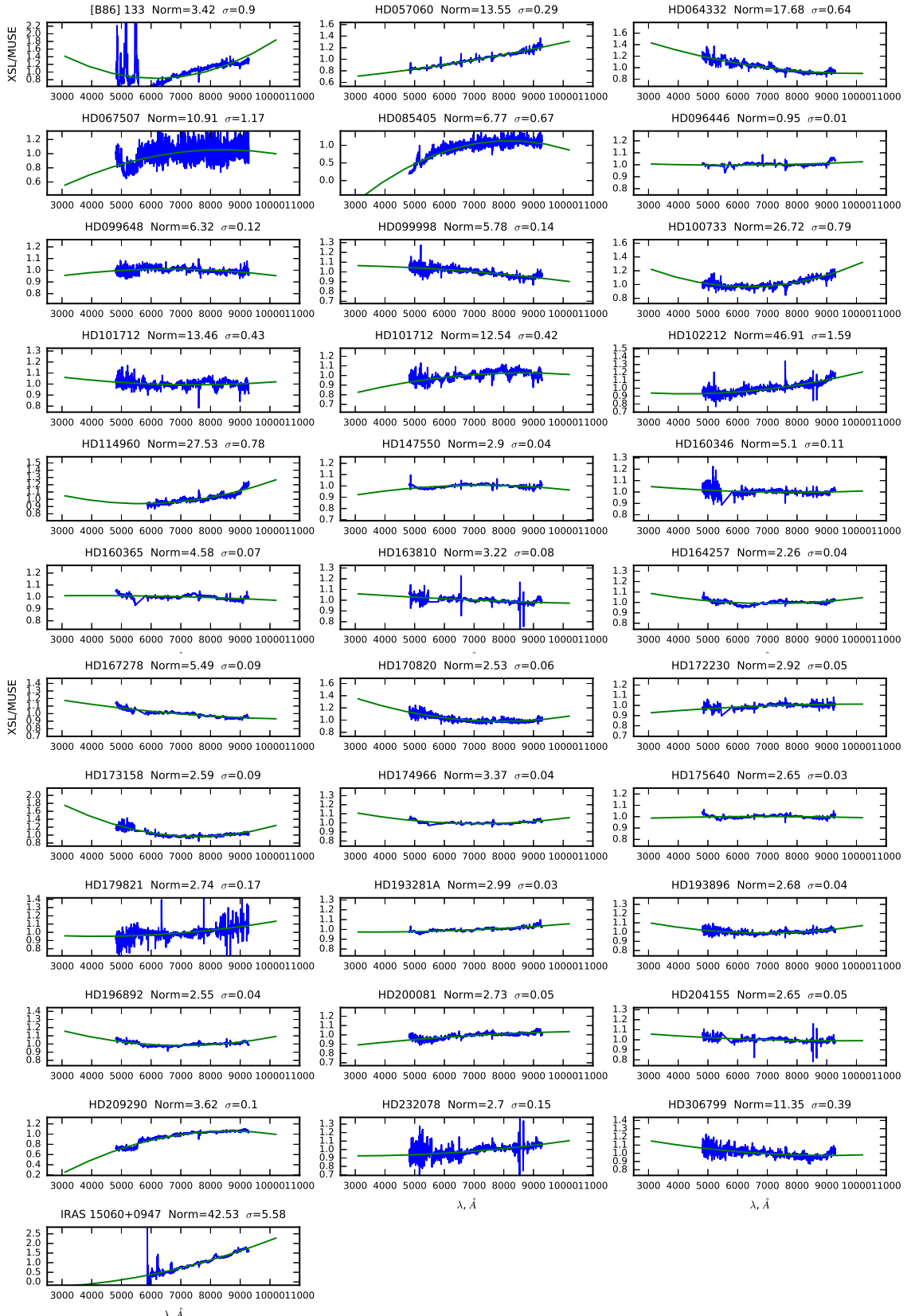


Fig. 4: Ratios of the XSL spectra to our MUSE spectra (blue; covers only the MUSE wavelength range), normalized to unity and median smoothed for display purposes with a 5-element wide median filter. Two ratios are show for HD 101712 – for the two XSL spectra of this star. A second order polynomial fits spanning the wavelength of XSL is also shown in blue. The labels on the top of each panel contain the name of the object, the normalization factor that indicates the flux ratio of the independently flux-calibrated MUSE and XSL spectra, and a standard deviation of the fits residuals. The coefficients of polynomial fits are listed in Table B.1.

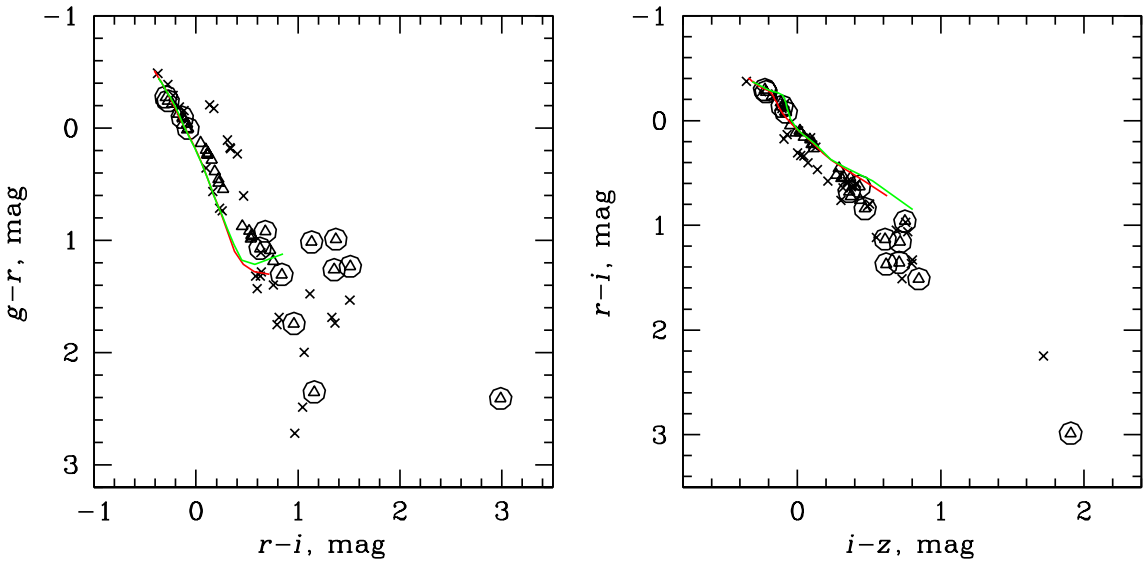


Fig. 5: Synthetic SDSS color-color diagrams derived from the MUSE (open circles) and XSL (open triangles) spectra. Larger open circles mark known variables, according to the SIMBAD database, and although many stars are variable, some distinct outliers are not. Sequences for Solar abundance dwarfs (red line) and giant (green line) stars from Lenz et al. (1998) are also shown. The extreme red outliers are IRAS 15060+0947 (V* FV Boo) – a known Mira variable. There are two points for this object on the right panel – they correspond to the XSL and the MUSE spectra.

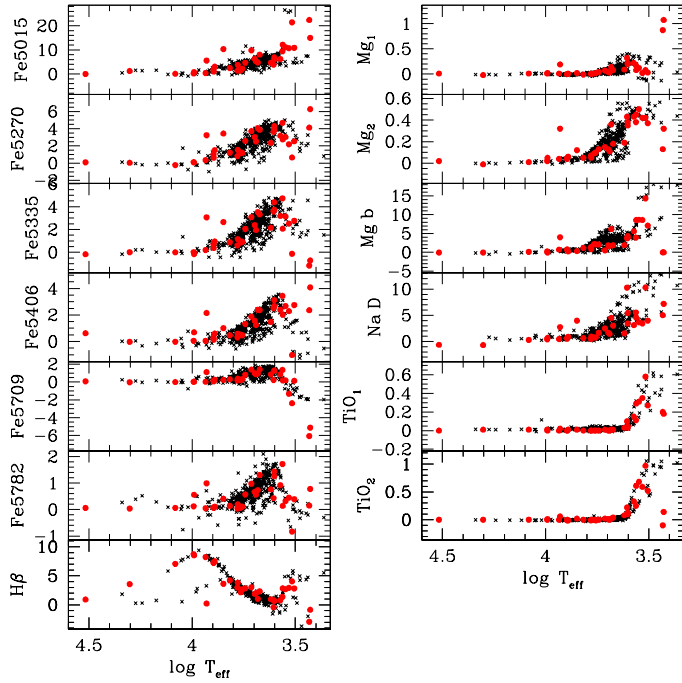


Fig. 6: Lick indices for the stars in our sample (red dots) and in the sample of Worley et al. (1994, black dots). Following their definitions, Mg_1 , Mg_2 , TiO_1 and TiO_2 are in magnitudes, and the rest are equivalent widths in units of Å. The two coldest objects that often deviate from the M-star dominated sequences are the carbon stars HD 067507 and HD 085405.

Appendix A: MUSE spectra.

Table A.1 presents the log of our MUSE observations and Fig. A.1 – the MUSE spectra.

Appendix B: Comparison with the XSL spectra.

Table B.1 lists the coefficients of polynomial fits to the ratios of the XSL spectra to our MUSE spectra. For further details see Sec. 4.

Appendix C: Lick indices from the MUSE spectra.

Table C.1 shows the Lick indices measured on our MUSE spectra.

Table A.1: Observing log. Six exposures were taken for all target except for HD 204155 which was observed 12 times. The UT date and time at the start of the first exposure is listed, together with the airmass range for the entire sequence and the exposure time of each individual spectrum.

ID (1)	Alternative ID (2)	RA DEC (J2000) (3)	UT start, yyyy-mm-dd hh:mm (4)	sec z dex (5)	Exp. sec (6)	Specphot. Std. (7)	sec z dex (8)
HD 057060	...	07:18:40.38 -24:33:31.3	2017-05-03 01:07	1.63-1.70	0.14	LTT 3218	1.01
HD 064332	...	07:53:05.27 -11:37:29.4	2017-05-03 01:23	1.61-1.68	4.80	LTT 3218	1.01
HD 067507	RU Pup	08:07:29.83 -22:54:45.3	2017-05-03 02:00	1.68-1.76	7.68	LTT 3218	1.01
HD 085405	Y Hya	09:51:03.72 -23:01:02.3	2017-05-03 02:17	1.21-1.23	1.94	LTT 3218	1.01
HD 096446	...	11:06:05.82 -59:56:59.6	2017-05-03 01:41	1.24-1.24	1.94	LTT 3218	1.01
HD 099648	...	11:27:56.24 +02:51:22.6	2017-07-18 23:54	1.89-2.00	0.14	GD 153	1.58
HD 099998	BS 4432	11:30:18.89 -03:00:12.6	2017-05-03 00:39	1.10-1.09	0.15	LTT 3218	1.01
HD 100733	BS 4463	11:35:13.28 -47:22:21.3	2017-05-02 06:55	2.39-2.52	0.95	GD 108	1.06
HD 306799	CD -60 3636	11:36:34.84 -61:36:35.2	2017-05-02 23:17	1.38-1.37	3.86	GD 108	1.06
HD 101712	...	11:41:49.41 -63:24:52.4	2017-04-18 06:59	1.84-1.89	4.79	EG 274	1.06
HD 102212	BS 4517	11:45:51.56 +06:31:45.7	2017-05-03 00:53	1.20-1.19	0.15	LTT 3218	1.01
HD 114960	...	13:13:57.57 +01:27:23.2	2017-04-01 07:35	1.35-1.39	1.93	GD 108	1.23
IRAS 15060+0947	...	15:08:25.77 +09:36:18.2	2017-07-18 23:35	1.22-1.21	43.65	GD 153	1.58
HD 147550	...	16:22:38.90 -02:04:47.5	2017-05-21 04:53	1.08-1.08	1.95	LTT 7987	1.03
HD 160365	...	17:38:57.85 +13:19:45.3	2017-05-21 08:33	1.53-1.57	1.92	LTT 7987	1.03
HD 160346	...	17:39:16.92 +03:33:18.9	2017-05-21 06:06	1.14-1.14	1.94	LTT 7987	1.03
HD 163810	...	17:58:38.45 -13:05:49.6	2017-05-21 08:51	1.18-1.21	14.56	LTT 7987	1.03
HD 164257	...	18:00:07.32 +06:33:14.1	2017-05-21 09:07	1.45-1.49	1.92	LTT 7987	1.03
[B86] 133	NSV 24166	18:03:45.47 -30:03:00.7	2017-05-02 07:11	1.03-1.02	83.77	GD 108	1.06
HD 167278	...	18:14:33.65 +00:10:32.9	2017-05-21 09:22	1.35-1.39	7.72	LTT 7987	1.03
HD 170820	...	18:32:13.11 -19:07:26.3	2017-05-28 09:43	1.31-1.32	3.87	LTT 7987	1.08
HD 172230	...	18:38:54.95 +06:16:14.8	2017-05-31 05:09	1.28-1.26	3.87	GD 153	1.48
HD 173158	...	18:43:45.31 +05:44:14.6	2017-05-31 05:25	1.25-1.23	6.78	GD 153	1.48
HD 174966	...	18:53:07.83 +01:45:19.7	2017-05-31 05:41	1.19-1.17	4.85	GD 153	1.48
HD 175640	...	18:56:22.66 -01:47:59.5	2017-05-21 09:36	1.23-1.26	1.94	LTT 7987	1.03
HD 179821	...	19:13:58.61 +00:07:31.9	2017-05-31 05:56	1.18-1.17	7.76	GD 153	1.48
HD 232078	...	19:38:12.07 +16:48:25.6	2017-05-31 07:12	1.35-1.34	9.67	GD 153	1.48
HD 193256	...	20:20:26.57 -29:11:28.8	2017-05-31 06:10	1.16-1.14	1.95	GD 153	1.48
HD 193281A	...	20:20:27.88 -29:11:50.0	2017-05-31 06:10	1.16-1.14	1.95	GD 153	1.48
HD 193281B	...	20:20:28.07 -29:11:47.2	2017-05-31 06:10	1.16-1.14	1.95	GD 153	1.48
HD 193896	...	20:23:00.79 -09:39:17.0	2017-05-31 06:25	1.19-1.17	1.94	GD 153	1.48
HD 196892	...	20:40:49.38 -18:47:33.3	2017-05-31 06:42	1.15-1.13	7.78	GD 153	1.48
HD 200081	...	21:01:22.42 -02:30:50.4	2017-05-31 06:55	1.28-1.25	6.77	GD 153	1.48
HD 204155	...	21:26:42.91 +05:26:29.9	2017-05-31 07:26	1.37-1.29	7.72	GD 153	1.48
HD 209290	...	22:02:10.27 +01:24:00.8	2017-05-31 07:56	1.33-1.30	9.66	GD 153	1.48

Table A.2: MUSE spectra of the program stars. Only ten entries for a few spectra are shown for guidance. The full spectra are available in the electronic edition.

λ (1)	$F_\lambda, \sigma(F_\lambda)$ erg cm $^{-1}$ s $^{-1}$ Å $^{-1}$ (2)
[B86] 133	
4750.351	9.0321e-15 1.3444e-16
4751.601	9.2171e-15 1.7869e-16
4752.851	9.1116e-15 1.3160e-16
4754.101	9.0764e-15 1.4030e-16
4755.351	9.3078e-15 1.4568e-16
...	
HD 057060	
4749.690	6.2487e-11 9.8514e-13
4750.940	6.6745e-11 9.7720e-13
4752.190	6.7090e-11 8.6972e-13
4753.440	6.6901e-11 9.2688e-13
4754.690	6.7012e-11 9.6207e-13
...	

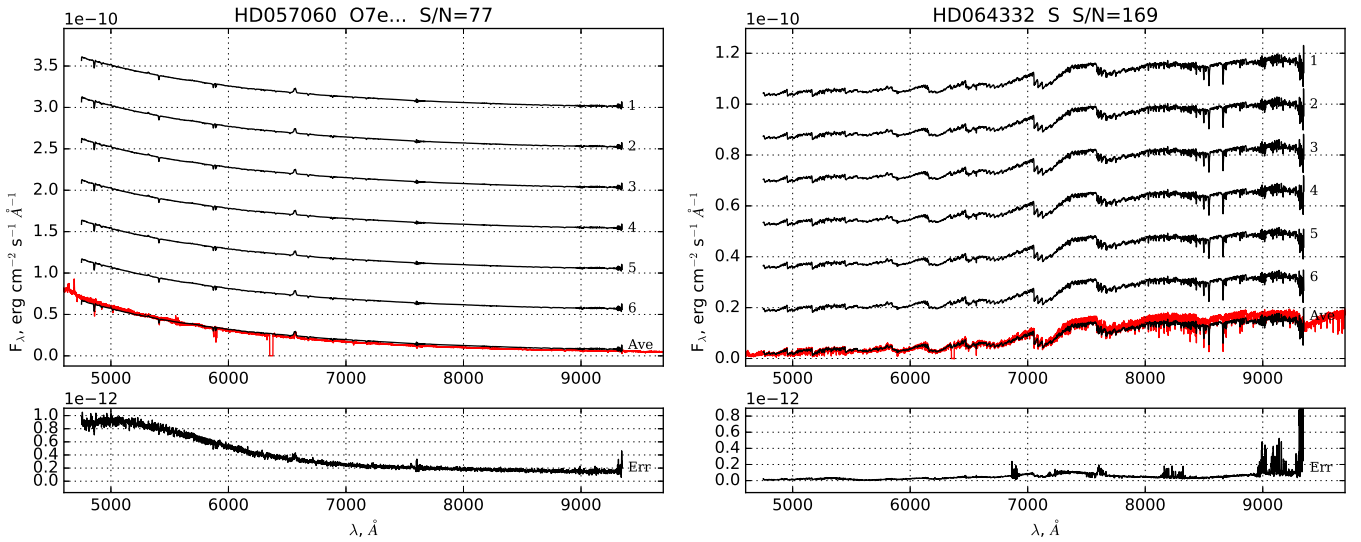


Fig. A.1: MUSE spectra (labelled on the top of each panel). The upper sub-panels show the spectra extracted from each individual exposure (shifted up for clarity) and the average spectra of the object at its true flux level. The XSL spectra, when available, are plotted with red underneath the averaged MUSE spectrum. The bottom sub-panels show the standard deviation of the average spectrum. The spectra of the other stars are presented in the electronic edition only.

Table B.1: Coefficients and their errors of second order polynomial fits to the ratios of the XSL spectra to our MUSE spectra: $Ratio = a_0 + a_1 \times \lambda + a_2 \times \lambda^2$. The standard deviation of the residuals σ is also listed.

ID (1)	a_0 (2)	a_1 (3)	a_2 (4)	σ (5)
[B86] 133	$1.0875e+01 \pm 4.9106e-01$	$-2.6034e-03 \pm 1.4250e-04$	$2.1119e-07 \pm 1.0070e-08$	$8.9657e-01$
HD 057060	$7.7783e+00 \pm 1.5925e-01$	$4.1637e-04 \pm 4.6240e-05$	$5.4824e-08 \pm 3.2693e-09$	$2.9142e-01$
HD 064332	$3.5697e+01 \pm 3.4877e-01$	$-3.9873e-03 \pm 1.0127e-04$	$2.0084e-07 \pm 7.1597e-09$	$6.3832e-01$
HD 067507	$-2.1863e+00 \pm 6.3861e-01$	$3.2643e-03 \pm 1.8542e-04$	$-1.9423e-07 \pm 1.3110e-08$	$1.1688e+00$
HD 085405	$-2.1686e+01 \pm 3.6461e-01$	$7.1684e-03 \pm 1.0587e-04$	$-4.3791e-07 \pm 7.4850e-09$	$6.6732e-01$
HD 096446	$9.9209e-01 \pm 7.7207e-03$	$-1.4847e-05 \pm 2.2418e-06$	$1.3103e-09 \pm 1.5850e-10$	$1.4131e-02$
HD 099648	$5.1713e+00 \pm 6.3635e-02$	$3.6673e-04 \pm 1.8477e-05$	$-2.7750e-08 \pm 1.3064e-09$	$1.1647e-01$
HD 099998	$6.1662e+00 \pm 7.5652e-02$	$3.3898e-05 \pm 2.1966e-05$	$-1.2490e-08 \pm 1.5530e-09$	$1.3847e-01$
HD 100733	$5.1682e+01 \pm 4.3041e-01$	$-8.1477e-03 \pm 1.2497e-04$	$6.4140e-07 \pm 8.8351e-09$	$7.8776e-01$
HD 101712	$1.6022e+01 \pm 2.3634e-01$	$-7.1526e-04 \pm 6.8618e-05$	$4.8079e-08 \pm 4.8512e-09$	$4.3258e-01$
HD 101712	$6.7516e+00 \pm 2.2716e-01$	$1.4180e-03 \pm 6.5952e-05$	$-8.2102e-08 \pm 4.6627e-09$	$4.1578e-01$
HD 102212	$5.0144e+01 \pm 8.6927e-01$	$-3.0969e-03 \pm 2.5240e-04$	$3.6520e-07 \pm 1.7845e-08$	$1.5910e+00$
HD 114960	$4.0233e+01 \pm 9.7355e-01$	$-5.0542e-03 \pm 2.5999e-04$	$4.4436e-07 \pm 1.7128e-08$	$7.8302e-01$
HD 147550	$2.1748e+00 \pm 2.1553e-02$	$2.0414e-04 \pm 6.2580e-06$	$-1.4080e-08 \pm 4.4245e-10$	$3.9450e-02$
HD 160346	$5.7738e+00 \pm 6.3278e-02$	$-1.7415e-04 \pm 1.8292e-05$	$1.1002e-08 \pm 1.2900e-09$	$1.1465e-01$
HD 160365	$4.5644e+00 \pm 3.9193e-02$	$3.6423e-05 \pm 1.1329e-05$	$-4.6190e-09 \pm 7.9902e-10$	$7.1011e-02$
HD 163810	$3.6215e+00 \pm 4.3395e-02$	$-7.4719e-05 \pm 1.2544e-05$	$2.6363e-09 \pm 8.8470e-10$	$7.8619e-02$
HD 164257	$2.9161e+00 \pm 2.1773e-02$	$-1.9122e-04 \pm 6.3208e-06$	$1.3446e-08 \pm 4.4681e-10$	$3.9867e-02$
HD 167278	$7.6624e+00 \pm 5.1776e-02$	$-4.5347e-04 \pm 1.4967e-05$	$2.0024e-08 \pm 1.0555e-09$	$9.3807e-02$
HD 170820	$5.0225e+00 \pm 3.4454e-02$	$-6.4631e-04 \pm 1.0002e-05$	$4.1002e-08 \pm 7.0704e-10$	$6.3086e-02$
HD 172230	$2.4422e+00 \pm 2.7921e-02$	$1.0172e-04 \pm 8.0709e-06$	$-5.0514e-09 \pm 5.6920e-10$	$5.0586e-02$
HD 173158	$8.3642e+00 \pm 4.7810e-02$	$-1.5581e-03 \pm 1.3820e-05$	$1.0331e-07 \pm 9.7467e-10$	$8.6622e-02$
HD 174966	$4.5597e+00 \pm 1.9866e-02$	$-3.4119e-04 \pm 5.7425e-06$	$2.3893e-08 \pm 4.0499e-10$	$3.5995e-02$
HD 175640	$2.5360e+00 \pm 1.8827e-02$	$3.5332e-05 \pm 5.4655e-06$	$-2.5504e-09 \pm 3.8634e-10$	$3.4474e-02$
HD 179821	$2.8459e+00 \pm 9.0632e-02$	$-1.1607e-04 \pm 2.6310e-05$	$1.3874e-08 \pm 1.8598e-09$	$1.6596e-01$
HD 193281A	$2.9758e+00 \pm 1.7990e-02$	$-3.8776e-05 \pm 5.2226e-06$	$5.5744e-09 \pm 3.6918e-10$	$3.2940e-02$
HD 193896	$3.5954e+00 \pm 2.2904e-02$	$-2.7330e-04 \pm 6.6490e-06$	$1.9823e-08 \pm 4.7000e-10$	$4.1936e-02$
HD 196892	$3.9280e+00 \pm 2.3032e-02$	$-4.0473e-04 \pm 6.6862e-06$	$2.8704e-08 \pm 4.7263e-10$	$4.2171e-02$
HD 200081	$2.0961e+00 \pm 2.5504e-02$	$1.2569e-04 \pm 7.4035e-06$	$-5.3440e-09 \pm 5.2332e-10$	$4.6702e-02$
HD 204155	$3.0281e+00 \pm 2.9675e-02$	$-8.6000e-05 \pm 8.5776e-06$	$4.6207e-09 \pm 6.0491e-10$	$5.3764e-02$
HD 209290	$-3.2922e+00 \pm 5.5030e-02$	$1.6589e-03 \pm 1.5975e-05$	$-9.6328e-08 \pm 1.1292e-09$	$1.0076e-01$
HD 232078	$2.5877e+00 \pm 8.0086e-02$	$-5.7710e-05 \pm 2.3251e-05$	$9.4294e-09 \pm 1.6436e-09$	$1.4658e-01$
HD 306799	$1.5678e+01 \pm 2.1450e-01$	$-1.0232e-03 \pm 6.2275e-05$	$5.6597e-08 \pm 4.4024e-09$	$3.9253e-01$
IRAS 15060+0947	$-1.0062e+01 \pm 7.1662e+00$	$-4.3525e-03 \pm 1.9079e-03$	$1.4548e-06 \pm 1.2536e-07$	$5.5817e+00$

HD114960	6.93±0.16	4.31±0.10	4.38±0.10	3.12±0.08	1.28±0.05	1.44±0.03	0.74±0.04	0.221±0.002	0.380±0.003	4.31±0.10	5.43±0.04	0.035±0.001	0.104±0.002
HD147550	0.24±0.20	0.13±0.02	0.01±0.01	0.05±0.02	0.02±0.05	0.12±0.05	8.72±0.08	0.009±0.001	0.021±0.002	0.26±0.05	0.42±0.09	0.008±0.002	0.004±0.002
HD160346	4.80±0.15	4.06±0.09	3.53±0.09	2.40±0.07	0.95±0.01	0.73±0.03	1.04±0.08	0.138±0.002	0.360±0.002	6.17±0.08	4.52±0.06	0.010±0.002	0.017±0.002
HD160365	3.75±0.09	1.54±0.12	1.16±0.14	0.59±0.11	0.37±0.04	0.20±0.06	3.80±0.06	0.001±0.002	0.049±0.002	0.84±0.11	0.92±0.11	0.003±0.003	0.000±0.002
HD163810	1.46±0.15	1.16±0.07	0.84±0.07	0.51±0.06	0.20±0.06	0.06±0.06	2.14±0.07	0.011±0.001	0.086±0.002	2.20±0.06	0.77±0.09	0.003±0.002	-0.000±0.002
HD164257	0.84±0.24	0.08±0.04	-0.15±0.07	0.69±0.07	0.03±0.09	0.56±0.09	8.53±0.05	0.017±0.002	0.048±0.002	-0.07±0.05	0.68±0.12	0.001±0.003	0.009±0.001
HD167278	2.48±0.11	1.22±0.08	0.89±0.10	0.47±0.10	0.31±0.06	0.14±0.04	4.21±0.03	-0.006±0.001	0.045±0.001	1.16±0.05	0.64±0.03	0.004±0.001	-0.001±0.001
HD170820	8.07±0.17	3.87±0.14	3.32±0.15	2.37±0.14	1.40±0.13	1.31±0.13	2.32±0.06	0.083±0.002	0.185±0.003	1.90±0.13	3.04±0.17	0.011±0.004	0.042±0.002
HD172230	3.10±0.07	1.52±0.06	0.95±0.07	0.60±0.06	0.25±0.05	0.11±0.04	7.50±0.03	0.015±0.001	0.056±0.001	0.25±0.06	0.88±0.04	0.006±0.001	-0.005±0.001
HD173158	9.86±0.07	3.73±0.05	3.09±0.08	1.88±0.09	1.38±0.06	0.98±0.04	3.04±0.03	0.069±0.001	0.146±0.001	0.52±0.02	2.50±0.04	0.009±0.001	0.024±0.001
HD174966	1.85±0.18	1.02±0.10	0.67±0.09	0.27±0.07	0.14±0.03	0.08±0.04	7.21±0.05	-0.003±0.002	0.043±0.002	0.68±0.10	0.64±0.07	0.004±0.002	-0.007±0.002
HD175640	0.14±0.17	-0.22±0.11	-0.00±0.11	-0.02±0.08	-0.01±0.03	0.06±0.04	7.05±0.05	0.008±0.002	0.010±0.002	0.11±0.10	0.28±0.07	0.006±0.002	-0.001±0.001
HD179821	10.34±0.11	3.44±0.06	2.66±0.05	1.01±0.03	0.24±0.03	0.41±0.03	3.61±0.04	0.023±0.001	0.123±0.002	0.31±0.07	3.97±0.05	0.010±0.001	0.017±0.001
HD193256	0.99±0.16	0.64±0.08	0.38±0.09	0.14±0.08	0.07±0.07	0.06±0.06	7.28±0.05	0.004±0.002	0.045±0.002	0.76±0.07	0.53±0.09	0.004±0.002	-0.004±0.002
HD193281A	0.40±0.14	0.36±0.08	0.20±0.09	0.05±0.08	0.03±0.07	0.05±0.06	8.22±0.05	0.006±0.001	0.039±0.002	0.72±0.07	0.46±0.09	0.004±0.002	-0.004±0.002
HD193281B	5.55±2.43	3.24±1.13	3.06±1.18	2.15±0.97	1.11±0.74	0.99±0.67	0.21±1.13	0.189±0.026	0.325±0.032	3.98±1.13	2.74±0.91	0.019±0.020	0.057±0.017
HD193896	5.26±0.09	2.52±0.04	1.96±0.04	1.24±0.04	0.86±0.05	0.56±0.06	2.04±0.03	0.031±0.001	0.110±0.001	1.65±0.04	1.45±0.08	0.005±0.002	0.002±0.002
HD196892	1.40±0.16	0.83±0.07	0.61±0.08	0.30±0.06	0.17±0.03	0.04±0.02	2.98±0.08	0.014±0.002	0.068±0.002	1.41±0.08	0.48±0.02	0.002±0.000	-0.007±0.001
HD200081	4.69±0.19	2.57±0.08	2.06±0.07	1.32±0.05	0.81±0.04	0.57±0.04	2.83±0.08	0.036±0.002	0.127±0.002	2.05±0.09	1.67±0.06	0.004±0.001	0.003±0.002
HD204155	2.26±0.20	1.21±0.13	0.92±0.15	0.47±0.13	0.32±0.10	0.11±0.08	2.65±0.10	0.019±0.002	0.096±0.003	2.12±0.11	0.76±0.10	0.003±0.002	-0.006±0.002
HD209290	3.85±0.10	3.63±0.08	3.58±0.10	2.51±0.08	0.21±0.04	0.43±0.03	-0.43±0.05	0.322±0.001	0.430±0.002	3.77±0.06	10.27±0.03	0.098±0.001	0.220±0.001
HD232078	4.70±0.10	2.36±0.06	2.15±0.07	1.48±0.05	0.84±0.03	0.76±0.02	0.95±0.04	0.091±0.001	0.192±0.001	1.90±0.03	1.53±0.03	0.031±0.001	0.081±0.001
HD306799	9.47±0.12	4.66±0.09	4.73±0.09	3.44±0.09	1.35±0.06	1.72±0.02	1.36±0.06	0.174±0.002	0.376±0.002	3.90±0.07	5.52±0.05	0.106±0.002	0.255±0.002
IRAS 15060+0947	21.43±0.31	0.66±0.23	-0.12±0.28	-1.02±0.21	-2.38±0.17	-0.83±0.13	4.03±0.26	0.081±0.003	0.424±0.005	14.34±0.10	10.32±0.14	0.576±0.003	0.972±0.005